Confidential

A PET Detector With Parallax-free Compton Enhanced 3D Gamma Reconstruction

Abstract

We describe a novel concept for a PET detector module providing full 3D gamma reconstruction with high resolution over the total detector volume, free of parallax errors. The key components are a matrix of long YAP:Ce scintillator crystals and Hybrid Photodiodes with matched segmentation and integrated readout electronics. They read out the two ends of the scintillator package. Both excellent spatial (x,y,z) and energy resolution is obtained. The concept allows to enhance the gamma detection efficiency by reconstructing a significant fraction of Compton scattered events and can in principle be also applied to scintillators other than YAP:Ce.

1. Introduction

In medical imaging Positron Emission Tomographs (PET) provide quantitative measurements on the metabolism of internal organs and their biochemistry by *in vivo* measuring specific activities of positron emitting radio-nuclides (mainly ^{18}F fluoro-deoxyglucose FDG). Over the last 20 years of continuous development PET scanners have demonstrated a tremendous potential for cancer diagnosis and treatment.
The challenge for advanced PET instrumentation is to optimise the performance (spatial resolution, acceptance, and system sensitivity) at the lowest possible construction and operation cost. This is particularly true for whole body ring scanners.

In this perspective we propose a novel 3D-PET concept, which is expected to provide higher performance at comparable or lower cost than existing operational scanners or known prototypes under development elsewhere.

As will be described in detail in chapter 2, the detector concept provides a full 3-dimensional reconstruction of the two 511 keV gamma quanta emitted at the moment of the positron annihilation. The detector has a large Axial Field Of View (AFOV). The gamma reconstruction is free of any parallax error and results in a precise measurement of the Depth Of Interaction (DOI). In addition to the detection of the gamma quanta by photoelectric effect, also a substantial fraction of Compton scattered events can be exploited. This approach allows to increase the sensitivity of the scanner by a factor 3-4.
The proposed concept is made possible by the latest developments of advanced instrumentation, in particular single photon detectors, performed at CERN for the future Large Hadron Collider. The use of large area and highly pixelized Hybrid Photo Diodes (HPD) with enclosed VLSI self-triggering electronics allows for a cost efficient readout

of finely segmented arrays of scintillator crystals. CERN is equipped with facilities to develop and build high performance HPD detectors optimised for PET applications.

2. Principle of operation

We propose a PET detector module consisting of a stack of small scintillation crystals read out on both sides by proximity focused HPD. In a PET scanner the modules will be arranged as a ring around the sample to be measured. In the axial direction (z) the large length of the crystals (10 cm) result in a large AFOV.

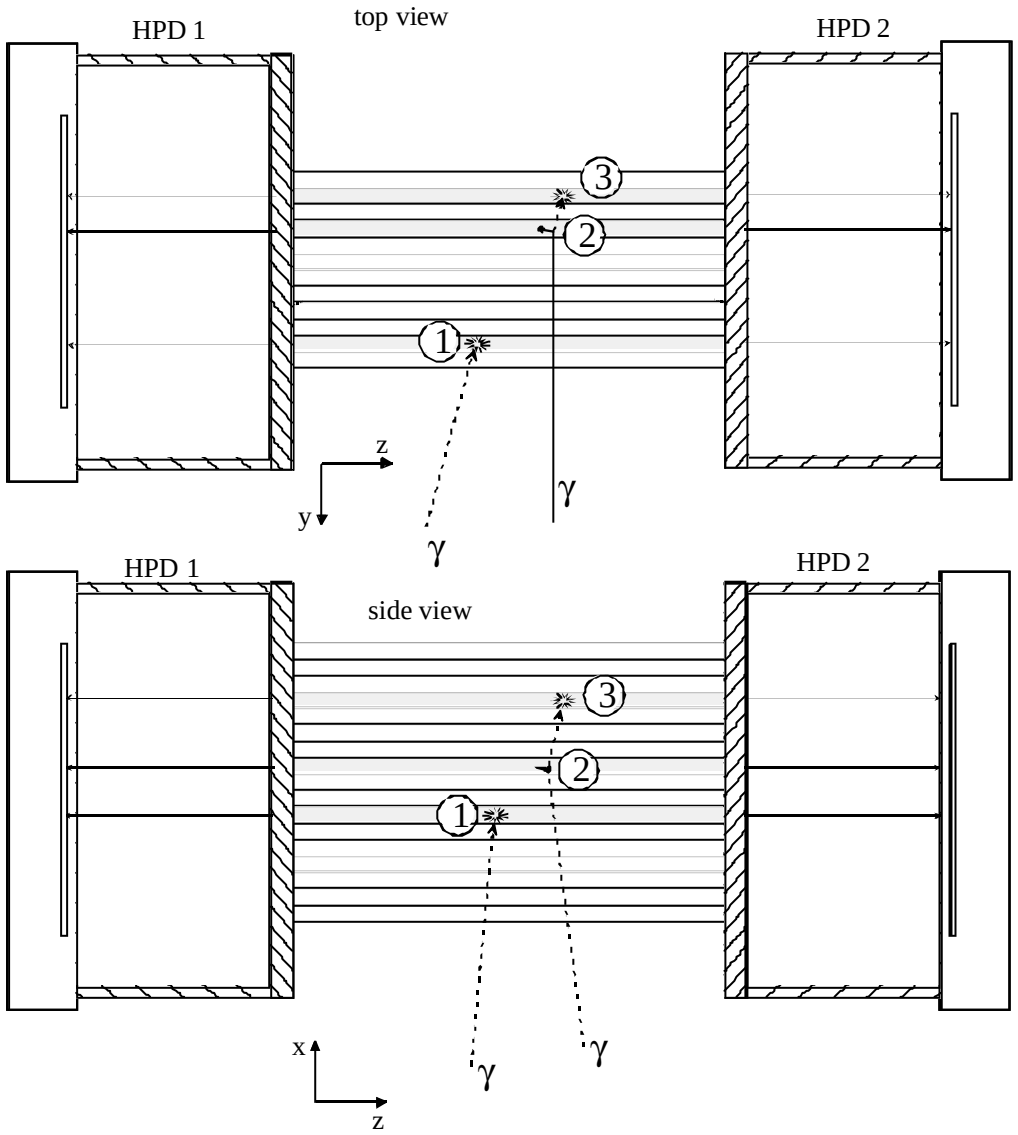

Figure 1: Schematic representation of one module of the PET detector. Two different detection modes for gammas are shown: The left gamma ray is converted by photoelectric effect ① . The right gamma ray undergoes first a Compton interaction ② and is finally absorbed by photoelectric effect ③ .

The thickness of the scintillator stack corresponds to about 3 absorption lengths. The segmentation of the detection volume in small bars and the matched segmentation of the silicon sensor of the HPD provide the required resolution in the x-y plane. The z coordinate is derived with high precision from the asymmetry of the amounts of light detected at the two ends of the scintillating crystals. Hence the interaction of the gamma ray is reconstructed in full 3D without any parallax error irrespective of the 511 keV gamma emission point.

The high light output of the scintillating crystals combined with the excellent energy resolution of the HPD results in a good energy measurement required for background discrimination. The short decay time constant of the scintillation light and the fast trigger output of the HPD readout electronics allow to define short coincidence intervals, which further reduces accidental background. The combination of 3D reconstruction of the gamma interaction point with the good energy resolution and the large detection volume provides another unique feature: In addition to the reconstruction of gammas by photoelectric effect, also a significant fraction of events which undergo single Compton scattering can be detected without degraded performance. This Compton enhanced mode increases very significantly the sensitivity of the detector.

3. Set-up

The key components of one module of the proposed PET detector comprise

- YAP:Ce scintillating crystals arranged in a rectangular matrix.
- Two segmented HPD detectors optically connected to the two extremities of the crystal matrix
- The front-end part of the self-triggering readout electronics is integrated in the vacuum envelope of the HPD.

Figure 1 shows a schematic representation of the set-up.

3.1 The scintillator matrix

A matrix of Cerium doped Yttrium Aluminium Perovskite (YAP:Ce) crystals serves as scintillation detector for the 511 keV gamma quanta. Among the commercially available crystals, YAP:Ce has been chosen for its good physical (see table 1) and mechanical properties. Cerium doped Lutetium Oxyorthosilicate (LSO:Ce) has comparable physical characteristics and the additional advantage of a large effective atomic number Z = 65. This leads to a higher probability for gamma conversion by photoelectric effect and therefore to a better detection efficiency. However LSO crystals of the required dimensions are currently not affordable and very difficult to fabricate.

For the performance estimates in chapter 4 we assume the crystals to have the following dimensions: 3.5 x 3.5 x 100 mm^3. Crystals of 100 mm length could be made by joining 2 or 3 shorter crystals with a glue of appropriate refractive index. All surfaces of the crystals are polished. The crystals are equally spaced in a rectangular matrix. Gaps of 0.3 mm between the crystals allow insertion of blinds (black paper). The light propagates

through the crystals by total internal reflection from the polished surfaces. The accepted solid angle, which is determined by the pair of refractive indices at the interface between crystals and photodetector windows (borosilicate glass, n = 1.474), is 17.5% of 4π towards both sides. The value of the bulk absorption length (14 cm) makes it possible to use long crystals and at the same time to obtain a significant light asymmetry required for the determination of the axial coordinate z

$$z = \frac{L}{2} \cdot \frac{Q_L - Q_R}{Q_L + Q_R},$$

with Q_L and Q_R being the charge signals measured at the left and right end of the crystal with total length L. In the following we consider a matrix of 12 by 18 crystals, as shown in figure 1.

Density r (g/cm^3)	5.55
Effective atomic charge Z	32
Scintillation light output (photons / MeV)	18000
Wavelength of max. emission (nm)	370
Refractive index n at 370 nm	1.94
Bulk light absorption length L_a (cm) at 370 nm	14
Principal decay time (ns)	27
mean γ attenuation length at 511 keV (mm)	22.4
mean γ absorption length at 511 keV (mm)	60.5

Table 1: Main characteristics of YAP:Ce scintillating crystals

3.2 The HPD detectors

The photodetectors, which are coupled to both ends of the crystal matrix, are Hybrid Photo Diode Detectors with flat entrance windows made of borosilicate glass. They are equipped with semi-transparent visible light bialkali photocathodes, which exhibit a quantum efficiency of about 25% at the wavelength of maximum emission 370 nm. The electron optics of the HPD is such that a 1:1 image of the photon pattern on the photocathode is transferred to the silicon sensor ("proximity focusing"). The silicon sensor is segmented into 216 individual diodes of dimensions 3.8 x 3.8 mm matching the pattern of the crystal matrix.
The HPD is operated at a moderate potential difference between photocathode and silicon sensor of about 12 kV. Photoelectrons impinging on the silicon sensor with an energy of 12 keV, produce on average about 3000 electron-hole pairs. In other words the internal gain of the HPD at 12 kV is about 3000. The point spread function, which describes the Gaussian width of the charge distribution on the silicon for a point like light source is of the order of 0.3 mm.

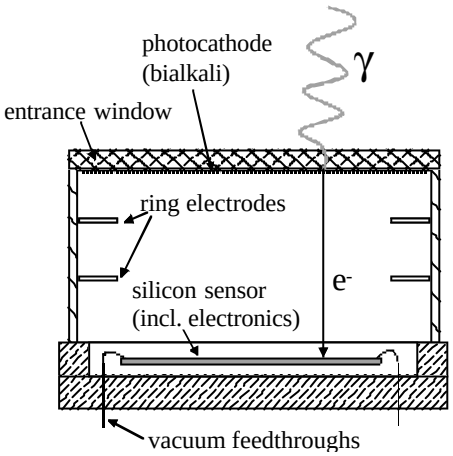

Figure 2: Schematic drawing of proximity focused HPD. The readout electronics (VATA-GP chip set) is encapsulated in the vacuum envelope.

The integrated self triggering electronics is mounted on a ceramic carrier which supports also the silicon sensor. We intend to use the VLSI chip VATA-GP, produced in 0.6 μ AMS CMOS technology. Each of the 128 channels of this chip has a charge integrating preamplifier, a shaper with a tuneable shaping time τ_s = 150 ± 50 ns and a readout register. A parallel fast shaper circuit (τ_s = 35 ns) produces a trigger signal for the readout logic. The chip features also a sparse readout option which allows to achieve event rates of the order of 100 kHz. The single photoelectron detection efficiency of the HPD with this electronics is expected to be 93%.

3.3 Integration of scintillator matrix and photodetectors

The scintillator matrix and the two HPD detectors form a module protected by a thin cover against external light. The individual YAP:Ce crystals are screened by sheets of black paper to avoid light propagation between crystals. The precise spacing of the crystals is ensured by 0.3 mm thick stainless steel wires, which are strung between the crystals close to the two ends of the matrix.

4 Expected Performance

To evaluate the expected performance of the above described detector module a number of analytical calculations have been performed, some of which have been supported by simple Monte Carlo simulations. A further improvement may be expected from a careful optimisation of the crystal dimensions.

4.1 Number of detected photons

The total number of detected photons N_{det} detected at both ends of the crystals is

$$N_{\det} = N_{ph} \cdot e_C \cdot e_Q \left(e^{-\frac{z}{L_a}} + e^{-\frac{L-z}{L_a}} \right)$$

The number of generated scintillation photons N_{ph}, following the absorption of a 511 keV gamma, is 0.511 MeV · 18,000 MeV^{-1} = 9200. The light transport efficiency e_C, ignoring bulk absorption, is 0.175, as described in section 3.1. The quantum efficiency at the wavelength 355 nm is 0.25. L_a denotes the bulk absorption length, z is the distance of the interaction point, measured from the end of the crystal with total length L.

Restricting to gamma reconstruction by photoelectric effect only, we expect for a 511 keV gamma

$$N_{\det} = 400 \cdot \left(e^{-\frac{z}{L_a}} + e^{-\frac{L-z}{L_a}} \right),$$

hence 596 reconstructed photons, if the interaction appears close to the bar end ($z = 0$) and 560 photons for z = 5 cm. The z-dependence of N_{det} is described by

$$N_{\det} = 591 - 7.23 \cdot z \quad 0 \le z(cm) \le 5$$

4.2 Energy resolution

The energy resolution $R = DE_{FWHM}/E$ is the quadratic convolution of three sources

$$R = R_{Sci} \oplus R_{stat} \oplus R_{noise}$$

The intrinsic resolution R_{sci} of the scintillator due to material in homogeneity, coupling between scintillator and photodetector and non-linear energy response has been measured to be 2.5%.

R_{stat} represents the statistical fluctuation involved in the light generation and detection process, including the photodetectors. $R_{stat} = 2.35/\sqrt{N_{rec}}$ The single stage dissipative gain mechanism of the HPD operated at 12 kV leads to a negligible contribution to R_{stat}.

Also the electronics noise R_{noise} of the detection chain is very small compared to the other two terms.

In summary, the energy resolution is nearly independent of the axial coordinate and can be approximated by

$$R \approx R_{stat} = \frac{2.35}{\sqrt{N_{rec}}} \approx 10\% \cdot \sqrt{\frac{511}{E_g\,(\mathrm{keV})}}$$

hence $R \approx 10\%$ (FWHM) at E_g = 511 keV and ≈ 22% at 100 keV.

4.3 Reconstruction of the interaction point

In the transverse x-y plane, the coordinates of the gamma interaction point in the scintillator are derived from the address of the hit crystal. The resolution is in first approximation determined by the dimensions of the crystals

$$s_x = s_y = \frac{s}{\sqrt{12}}$$

with s = 3.5 mm being the size of the crystals in the transverse direction. The spatial resolution of the HPD is matched to this value and will not contribute significantly. Hence the x and y coordinate of the gamma interaction can be reconstructed with a precision of better than 2.5 mm (FWHM).

The axial z coordinate is derived from the measurement of the asymmetry of the amount of light (= charge) detected at the two sides of the crystal.

$$z = \frac{L}{2} A_Q \qquad A_Q = \frac{Q_R - Q_L}{Q_R + Q_L}$$

By error propagation the precision s_z is derived to

$$s_z = \frac{L}{Q}\left(Q_L s_{Q_R} \oplus Q_R s_{Q_L}\right) \qquad Q = Q_R + Q_L$$

Ignoring electronics noise and assuming perfect linearity of the HPD charge signal and the number of reconstructed photons, the charge uncertainties are

$$s_{Q_{R,L}} = \sqrt{N_{rec_{R,L}}}$$

This leads to a resolution in the coordinate ranging from s_z/L = 2.1% in the middle of the crystal (z = 5 cm) to s_z/L = 1.9% at the ends. For the discussed geometry (L = 10 cm) the z coordinate of a 511 keV gamma can be reconstructed with a precision of better than 5 mm (FWHM). For 100 keV the precision is of the order 10 mm (FWHM).

4.4 Electronic response and time resolution

The electronics noise of the VATA-GP electronics is of the order 500 e^- ENC. The dynamic range of the HPD electronic readout chain has to be 80. This is driven by

- the expected maximum number of photons: ca. 400 for the conversion of gamma with 511 keV energy close to the end of crystal
- and the detection threshold of the fast trigger circuit used for the timing: we assume a threshold corresponding to 5 photons, which is equivalent to an energy deposit of 6.4 keV or 15,000 e^- created in the silicon.

The detection threshold of 15,000 e^- provides very comfortable and clean working conditions as it is a factor 30 above the electronics noise.
The time walk of the fast trigger circuit between gamma at 511 keV (400 photons) and one at 50 keV (50 photons) can be estimated in first approximation:

$$\Delta t = N_{thr}^{ph} \cdot t_{peak} \left(\frac{1}{N_{511keV}^{ph}} - \frac{1}{N_{50keV}^{ph}} \right)$$

With a peaking time t_{peak} of 35 ns we find a time walk *Dt* of less than 3.5 ns, which is comparable to classical PMT based systems.

4.5 Detection efficiency with Compton enhancement

YAP:Ce is a scintillating crystal in the medium Z range. Consequently the probability for photoelectric conversion of a gamma at 511 keV is only e_g^{photo} = 4%. Hence the probability to convert both 511 keV quanta by photoelectric effect is low.
The gamma reconstruction in full 3D and the large detection volume allow however to take into account a substantial fraction of events which underwent Compton scattering. The total energy is reconstructed by summing up the energies of all hit bars. To unambiguously distinguish between the coordinate of the primary Compton interaction (to be used in the tomographical reconstruction algorithm) and the coordinate of the final absorption of the photon, one has to restrict to events in which the photon is scattered into the forward hemisphere. The criteria for the event selection are derived from the Klein-Nishina formula, which describes the energy and angle dependent Compton cross-section

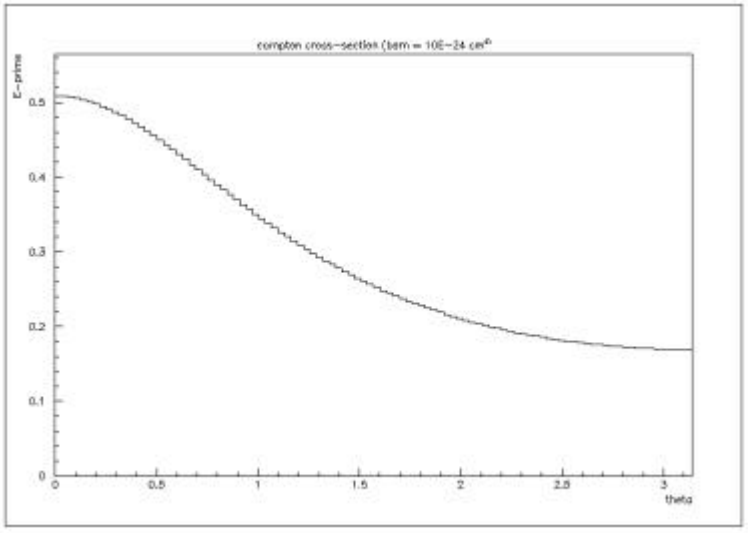

Figure 3: Compton kinematics. The plot shows the energy of the scattered photon versus the scattering angle (rad).

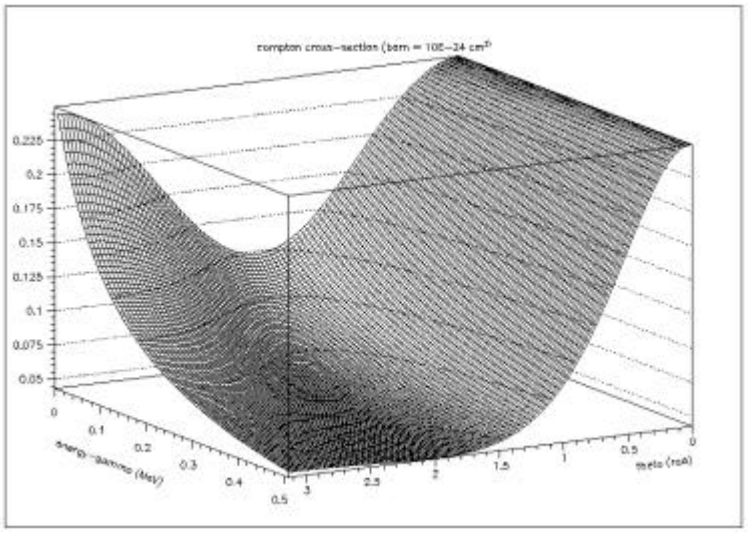

Figure 4: Cross-section for Compton scattering (Klein-Nishina formula) as a function of the initial photon energy and the scattering angle. In the classical low energy limit the total Compton cross-section reduces to the Thomson cross-section $s = \frac{8}{3} p r_e^2$.

and the Compton kinematics. Both are shown in figures 3 and 4.
A detailed analysis shows that a Compton scattering angle can be restricted to $0 \le \theta \le 60°$ (i.e. scattering into the forward hemisphere) if the energy deposit in the first interaction, seen from the centre of the PET scanner, is below 170 keV (for a gamma of 511 keV). 60% of all events fall in this category. The detection probability of one gamma involving both Compton and photoelectric effect is hence

$$e_g^{CE} = 0.6 \cdot e_g^{photo} = 2.4\%$$

The probability of the coincident Compton enhanced detection of two 511 keV gammas becomes

$$e_g^{CE} = 2 \cdot \left(0.6 \cdot e_g^{photo}\right) \cdot e_g^{photo} + \left(0.6 \cdot e_g^{photo}\right)^2 + \left(e_g^{photo}\right)^2 = 0.41\%$$

This result represents a sensitivity improvement of a factor 2.5 and can be considered as conservative estimate, since the increase of the photoconversion probability at lower gamma energies (E_g < 511 keV) has been neglected. The precise gain due to the Compton effect is under study using an adequate electromagnetic shower code.

5 Design of a Global PET system

A global PET scanner system can be built up from the detector modules described above in a straightforward way. In figure 5 an axial view of a ring scanner of 40 cm inner diameter is shown. In total 24 detector modules are required to provide a full crack free coverage of the circumference. The total number of crystals is 5184. They are read out by 48 HPD detectors. The total detection volume is 6350 cm^3.

Sensitivity and signal to noise ratio of the detector system

The system is equipped with a readout logic, which requires two orthogonal modules to fire within a coincidence time of t_{MS} = 10 ns, defined by the monostables of the VATA-GP3 chips. The random coincidence rate is given by

$$N_f = 2t_{MS} \cdot N_1 \cdot N_2$$

where $N_{1,2}$ are the counting rates of the two opposite detector modules. Requiring less than 1% random coincidences and assuming $N_1 = N_2$ limits the counting rate of one detector module to 500 kHz. Taking into account the solid angle defined by one detector module ($\Delta\Omega/4\pi$ = 0.87 %) this translates in a maximum activity of the positron source

$$A_{\max} = \frac{N}{\Delta\Omega} = 57 \text{ MBq} = 1.55 \text{ mCi}$$

which is comparable to the activity regulated by the international protocols for PET imaging. However as a result of the Compton enhanced reconstruction we expect a better signal to noise ratio for the same activity or, in other words, a PET image with higher contrast.

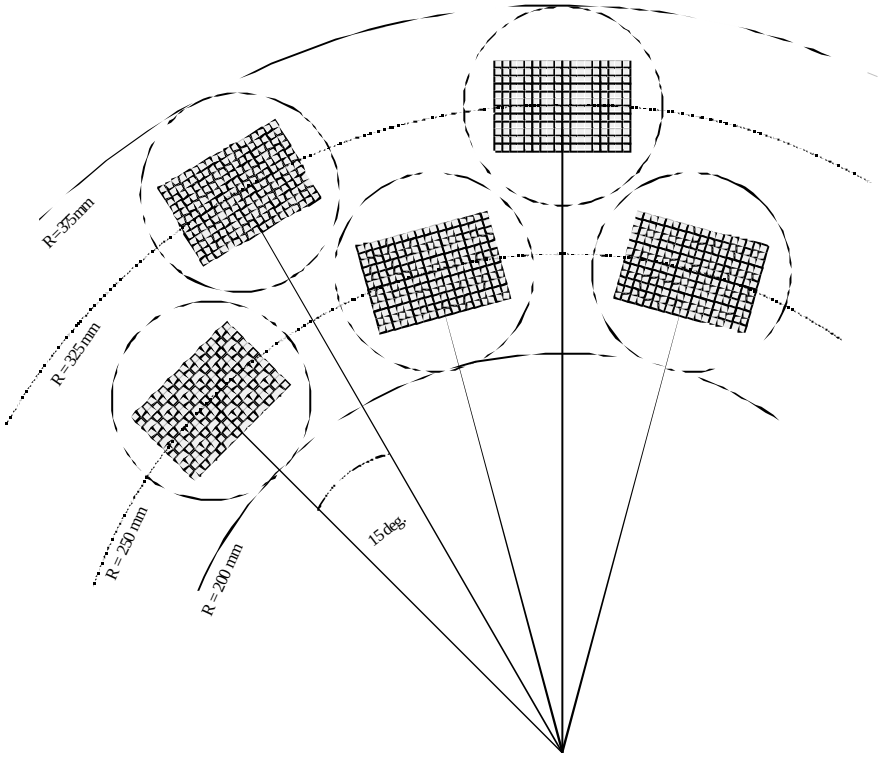

Fig. 5: Arrangement of 24 detector modules to a full PET ring scanner.

6 Comparison with existing systems

Conventional PET systems in use for medical applications employ gamma detectors consisting of several stacked rings of scintillating crystals to obtain a volumetric image. In 2D PET designs the rings are separated by tungsten septa such that only coincidences of opposite crystals within the ring or neighboured rings are recorded. In 3D designs these septa are suppressed and coincidences of crystals from all rings are registered.

The scintillator crystal, usually BGO blocks of 2" x 2" cross section are radially oriented and read out by 4 standard (i.e. position insensitive) 1" photo multiplier tubes. More recently also LSO crystals have been used in prototypes. The radial length of the crystals corresponds to about 3 absorption lengths, leading to absorption of 95% of the gamma quanta at 511 keV. In some designs equidistant crossed slots segment the scintillator blocks over a large fraction of their length into sub-crystals. This results in a better resolution of the projected photo-conversion point from the interpolated charge signals of the phototubes. The radial coordinate, i.e. the depth of interaction, is however not determined, leading to a degraded reconstruction precision due to parallax errors.

The parallax error problem, inherent to the above described detector geometry, has recently been addressed in several prototype developments:

- Phoswitch approach: Two or more blocks of different scintillator material with different time constant are piled up in radial direction. The time information is converted in a radial coordinate.
- Detector stacks: Several layers of 2D photon detectors are stacked to a 3D device
- Light sharing between the two opposite sides of the crystal.

The last approach, which is also employed in our design, has already been investigated and experimentally studies with commercially available photodetectors. In a recent project a matrix of LSO crystals was readout on one side by an array of PIN photodiodes and on the opposite side by a conventional PMT. Also avalanche photodiodes (APD) or multi-anode PMT were employed. However, each of these detectors exhibits intrinsic limitations (pixel size, number of pixels, surface coverage, energy resolution, gain uniformity), which compromise the final performance of the PET scanner.

7 Conclusions

We propose a novel parallax free 3D PET concept based on scintillator matrix structure readout on both sides by Hybrid Photodiodes. The concept allows building devices with large field of view. Compared with existing operational devices, a significantly higher detector performance is expected. The detector sensitivity is enhanced by reconstructing a sizable fraction of Compton scattered events. The concept could in principle also be implemented using a matrix of LSO scintillator crystals, where an even higher sensitivity could be achieved.